Zuo *et al. Molecular Cancer* (2025) 24:54
https://doi.org/10.1186/s12943-025-02248-3

Molecular Cancer

RESEARCH Open Access

Spatial transcriptomic analysis of tumor microenvironment in esophageal squamous cell carcinoma with HIV infection

Yuanli Zuo[1†], Yang Jin[1†], Gang Li[2†], Yue Ming[1], Ting Fan[1], Yitong Pan[1], Xiaojun Yao[2*] and Yong Peng[1*]

Abstract

Background Human Immunodeficiency Virus (HIV) is one of the most prevalent viruses, causing significant immune depletion in affected individuals. Current treatments can control HIV and prolong patients' lives, but new challenges have emerged. Increasing incidence of cancers occur in HIV patients. Esophageal squamous cell carcinoma (ESCC) is one of the most common cancers observed in HIV patients. However, the spatial cellular characteristics of HIV-related ESCC have not been explored, and the differences between HIV-ESCC and typical ESCC remain unclear.

Methods We performed spatial transcriptome sequencing on HIV-ESCC samples to depict the microenvironment and employed cell communication analysis and multiplex immunofluorescence to investigate the molecular mechanism in HIV-ESCC.

Results We found that HIV-ESCC exhibited a unique cellular composition, with fibroblasts and epithelial cells intermixed throughout the tumor tissue, lacking obvious spatial separation, while other cell types were sparse. Besides, HIV-ESCC exhibited an immune desert phenotype, characterized by a low degree of immune cell infiltration, with only a few $SPP1^+$ macrophages showing immune resistance functions. Cell communication analysis and multiplex immunofluorescence staining revealed that tumor fibroblasts in HIV-ESCC interact with $CD44^+$ epithelial cells via COL1A2, promoting the expression of PIK3R1 in epithelial cells. This interaction activates the PI3K-AKT signaling pathway, which contributes to the progression of HIV-ESCC.

Conclusions Our findings depict the spatial microenvironment of HIV-ESCC and elucidate a molecular mechanism in the progression of HIV-ESCC. This will provide us insights into the molecular basis of HIV-ESCC and potential treatment strategies.

Keywords Esophageal squamous cell carcinoma, HIV, Spatial transcriptome, Tumor microenvironment

[†]Yuanli Zuo, Yang Jin and Gang Li contributed equally to this work.

*Correspondence:
Xiaojun Yao
flyingyao@163.com
Yong Peng
yongpeng@scu.edu.cn

[1]Center for Molecular Oncology, Frontiers Science Center for Disease-Related Molecular Network, State Key Laboratory of Respiratory Health and Multimorbidity, State Key Laboratory of Biotherapy and Cancer Center, West China Hospital, Sichuan University, Chengdu 610041, China
[2]Department of Thoracic Surgery, The Public Health Clinical Center of Chengdu, Chengdu 610061, China

Background

Human Immunodeficiency Virus (HIV) is a retrovirus that compromises the human immune system by targeting and destroying crucial immune cells [1]. As a result, individuals infected with HIV are vulnerable to various opportunistic infections and malignancies, which can profoundly affect their overall health and pose life-threatening risks. The introduction of highly active antiretroviral therapy (HAART) has revolutionized the management of HIV, transforming it from a once-fatal disease into a manageable chronic condition. This advancement has significantly prolonged the lives of people living with HIV (PLWH). However, despite these progressions, the prevalence of chronic comorbidities within this population has emerged as a critical concern [2].

Currently, cancer has increasingly emerged as one of the leading causes of death among individuals living with HIV. The incidence of tumors in this population is markedly higher than in the general public. Furthermore, the interaction between HIV and various tumors poses considerable challenges in effectively treating patients affected by both conditions [3, 4]. In recent years, esophageal squamous cell carcinoma (ESCC) has been found to be one of the most common cancers in HIV-positive patients [5, 6].

Esophageal cancer is a prevalent malignant tumor, with ESCC accounting for over 80% of cases [7]. China is recognized as a high-incidence region for ESCC, comprising approximately half of the global population of affected patients [8]. The early symptoms of ESCC are often subtle, and clinical treatment outcomes are generally poor, contributing to a low five-year survival rate among patients [9]. Surgical resection remains one of the most effective methods for curing ESCC. However, the tumor's anatomical location can complicate surgery, resulting in significant surgical trauma and reduced patient tolerance. These factors consequently increase rates of surgical mortality and postoperative complications. Moreover, the pathological and physiological changes brought on by HIV infection can elevate the risk of opportunistic infections following surgery. Such complications may include wound infections, impaired wound healing, and anastomotic leaks [10]. In severely infected individuals, these issues can escalate to multiple organ failure and even death. As a result, there are notable differences in the clinical presentation and treatment approaches for ESCC associated with HIV compared to those without HIV infection.

However, research on ESCC with HIV infection (HIV-ESCC) remains limited, primarily due to the unique characteristics of this patient population. Only two earlier studies indicated that HIV infection is a risk factor affecting the prognosis of ESCC patients [11, 12]. Moreover, broader investigations into HIV-related tumors suggest that cancer patients with HIV generally experience poorer prognoses. For instance, Szychowiak et al. revealed that individuals with both HIV and cancer face higher mortality rates [13]. Similarly, Salahuddin et al. demonstrated that the prognosis for head and neck squamous cell carcinoma patients living with HIV is significantly worse compared to their non-HIV-associated counterparts, indicating that HIV serves as an independent predictor of adverse clinical outcomes [14].

The poor prognosis of patients with HIV-related tumors could be due to significant changes at the cellular and molecular levels. In patients with both HIV and lung cancer, there is a markedly higher frequency of microsatellite alterations and genomic instability [15]. Furthermore, compared to cancer patients who are not infected with HIV, those with HIV may experience declines in $CD4^+$ T cell counts and increased mortality rates as a result of chemotherapy and radiotherapy [16]. In addition, HIV infection is closely associated with elevated PD-L1 expression in liver cancer cells and the surrounding tumor microenvironment, which contributes to a highly immune-exhausted state. This condition alters the functions of cytotoxic and regulatory T cells and disrupts pro-inflammatory pathways, ultimately impacting the efficacy of immunotherapy [17]. Despite these findings, there lacks the study to explore the molecular mechanisms underlying HIV-ESCC. Therefore, there is an urgent need to understand the cellular and molecular characteristics of HIV-ESCC. Such investigations could offer new insights and directions for the diagnosis and treatment of this complex condition.

Currently, spatial transcriptomics is an innovative technique employed to study gene expression across different tissue and cell types. Unlike traditional transcriptomic studies, which often homogenize tissue samples and consequently lose critical spatial information, spatial transcriptomics preserves this spatial context. This approach allows for a more comprehensive understanding of the heterogeneity and interactions among various cell types within the tumor microenvironment, providing new insights to improve cancer treatment strategies. Several studies have explored the application of spatial transcriptomics in ESCC. For example, Guo et al. integrated spatial transcriptomics with single-cell transcriptomics to reveal the distributional heterogeneity of various stromal cells and their subpopulations in ESCC [18]. Similarly, Liu et al. utilized spatial transcriptomics to identify key genes involved in the progression from precancerous lesions to malignant tumors in ESCC [19]. These findings indicate that employing spatial transcriptomics to investigate HIV-ESCC could illustrate the specific changes in the tumor microenvironment attributable to HIV infection, thus uncovering critical underlying mechanisms. Here, this study aims to leverage advanced spatial

transcriptomics sequencing technology to thoroughly explore the essential molecular mechanisms of HIV-ESCC at the spatial cellular level of tumor, highlighting the mechanistic differences between HIV-ESCC and non-HIV-associated ESCC.

Methods

Sample collection

Patients included in this study were recruited from The Public Health Clinical Center of Chengdu. The inclusion criteria were as follows: (1) patients who underwent surgical treatment without any prior neoadjuvant therapies such as chemotherapy, radiotherapy, or molecular targeted therapy; (2) individuals confirmed to be HIV-positive through standardized HIV diagnostic testing, with esophageal squamous cell carcinoma verified through preoperative and postoperative biopsies; (3) patients with no evidence of tumor metastasis; (4) aged between 18 and 95 years. Written informed consent was obtained from all participants involved in this study. Here, we selected two samples for spatial transcriptomic sequencing (Table S1).

Spatial transcriptome sequencing

Fresh tissue samples were embedded in pre-cooled OCT and stored at -80 °C. Sections were cryosectioned, assessed for RNA integrity (RIN ≥ 7), and stained with hematoxylin and eosin (H&E) for structural evaluation. Using the 10X Genomics Visium platform, tissue sections were permeabilized to optimize mRNA capture, with optimal conditions determined based on fluorescence signal quality. Library construction followed the Visium Spatial Gene Expression protocol, including reverse transcription, cDNA amplification and quality control. Sequencing was conducted on an Illumina NovaSeq 2000 system, achieving a depth of 50,000-100,000 reads per spot.

Raw data processing

Histological images were manually aligned using 10X Visium Loupe Browser (v4.0.0), marking spots with > 50% tissue content as tissue regions and others as background, to refine tissue boundaries. Alignment results were exported for processing with Space Ranger (v1.3.0; 10x Genomics). Raw FASTQ files, histological images and the JSON alignment file were aligned to the GRCh38 reference genome, generating the primary gene expression matrix. For details on Loupe Browser usage, see https://support.10xgenomics.com/spatial-gene-expression/software/visualization/latest/alignment; the reference genome can be downloaded from https://cf.10xgenomics.com/supp/spatial-exp/refdata-gex-GRCh38-2020-A.tar.gz.

Quality control and dimensionality reduction clustering

For the Gene-Spot matrix generated by Space Ranger, initial statistical analyses were conducted, including calculating the number of UMIs and genes detected in each spot. For each ST sample, spots with fewer than 200 detected genes or with over 20% mitochondrial gene expression were filtered out. The filtered data were then processed using stLearn [20], including gene filtering, total count normalization, log transformation, data centering, and PCA for dimensionality reduction (selecting the top 50 principal components). Subsequently, each valid spot's image area was extracted, and high-level features were obtained using deep learning. The SME (Spatial Morphological Extraction) normalization algorithm was then applied, smoothing gene expression values at each center spot based on the morphological similarity of its neighboring spots. This normalized data was further scaled and dimensionally reduced. Finally, a neighborhood graph (n_neighbors = 17) was constructed from the SME-normalized data, and Louvain clustering (resolution = 1.19) was performed. The results were visualized using a UMAP (Uniform Manifold Approximation and Projection) plot, which effectively displayed the spatial distribution of clusters.

Histopathological notes

In this study, pathologists annotated the H&E-stained images of the sequencing specimens. Based on the histomorphological characteristics of samples, they identified and delineated tumor tissue regions and adjacent normal tissue regions.

Inference of CNV

We inferred copy number variation (CNV) abnormalities based on disturbances in chromosomal gene expression. The inferCNV method was employed to estimate the CNV of each tumor spot according to its transcriptomic profile [21]. For each patient, spots annotated by pathologists as adjacent normal regions were defined as normal references. The gene expression count matrix served as the input, and CNV distribution was detected using inferCNV. Genes with an average count of 0.1 or less across spots were excluded. We set the parameter 'Cluster_by_groups' to True to examine CNV status within each cluster. Additionally, to facilitate a clearer assessment of CNV, the denoising option was applied. The results from inferCNV were visualized using heatmaps.

ESTIMATE

We used the R package ESTIMATE (v1.0.13) to estimate the presence of stromal and immune cells within tumor tissues. ESTIMATE utilizes 141 marker genes from immune cells and 141 marker genes from stromal cells to compute two enrichment scores: the ImmuneScore

and the StromalScore. Tumor purity was then calculated using the formula described by Yoshihara et al. (Eq. 1) [22]. Normalized expression data for each spatial feature were estimated to analyze the returned StromalScore, ImmuneScore, and tumor purity for each feature, which were subsequently visualized on spatial spots.

$$Tumor\ purity = \cos\left(\begin{matrix}0.6049872018 + 0.0001467884 \\ \times ESTIMATE\ score\end{matrix}\right) \quad (1)$$

Cell type signature score

We reviewed several studies on esophageal squamous cell carcinoma to collect classical marker genes for cell types within esophageal tissues, which were used for cell type annotation. At the current Visium ST resolution, each spot may contain approximately 8–20 cells, making it challenging to assign a precise cell type to each spot. Therefore, we utilized Seurat's AddModuleScore function to calculate the normalized weighted average expression of classical marker genes for each cell type. By examining the scoring of classical marker genes across clusters, we compared the relative enrichment of cell types in different clusters, facilitating cell type annotation.

Deconvolution of spatial data

We obtained scRNA-seq data of ESCC samples from the Sequence Read Archive database (accession number SRP327447) [23]. After preprocessing and dimensionality reduction of the raw data, cell types were annotated based on classic marker genes we collected. We then used the CARD [24] package in R to perform spatial deconvolution of cell types. Using CARD_deconvolution, cell-type proportions were generated for each spatial spot, based on references from the scRNA-seq data. Visualization of these results with CARD.visualize.pie displayed the distribution of cell types across spatial spots.

Cell-cell interaction analysis

We used the CellChat [25, 26] package in R to evaluate cell-cell communication between different clusters in the sample. CellChat initially builds an intercellular communication network by identifying ligand-receptor (LR) pairs based on known interactions. For each cluster, CellChat quantifies the strength and probability of these interactions, thus modeling the communication pathways active between clusters. Then we employed stLearn [20] to assess the significance of LR signaling within spatial spots. We detected LR pairs within spots by setting a filter threshold of at least 20 detectable pairs per spot. To evaluate statistical significance, we performed permutation testing with 10,000 randomly generated gene pairs (n_pairs = 10000).

Differentially gene expression

To compare the differential genes between spots with significant COL1A2-CD44 interactions and those without, we used Seurat FindMarkers function to calculate the log2 fold change (log2FC) between the two groups. The Wilcoxon test and Bonferroni correction were applied to determine the significance of the differences. Genes were selected as differentially expressed based on the following statistical thresholds: average log2 fold change (avg_log2FC) > 1, p-value < 0.01, and adjusted p-value (Bonferroni) < 0.01, with an expression proportion greater than 25% in either group. The differentially expressed genes were visualized using a volcano plot.

KEGG pathway enrichment analysis

Significantly over-expressed genes were used as the input gene list for enrichment analysis, with the Kyoto Encyclopedia of Genes and Genomes (KEGG) serving as the gene function annotation source. The clusterProfiler package was utilized for gene enrichment analysis. First, the bitr() function was used to convert GeneSymbols to EntrezIDs. Then, the enrichGO() and enrichKEGG() functions were applied to perform GO functional enrichment analysis and KEGG pathway enrichment analysis on the differentially expressed genes, respectively. Finally, significantly enriched molecular signaling pathways were identified based on a threshold of p.adj ≤ 0.05.

Survival analysis

To evaluate the impact of COL1A2 on the prognosis of ESCC, we obtained RNA-seq and clinical data of ESCC samples from the TCGA database. Tumor samples were divided into two groups based on the average expression level of COL1A2. Survival curves were fitted using the Kaplan-Meier method from the 'Survival' R package, and visualized with the ggsurvplot function from the 'survmine' R package.

Multiplex immunofluorescence

We performed multiplex immunofluorescence on HIV-ESCC tissue samples to investigate the presence of mixed epithelial and fibroblast cells, and to examine the interaction between fibroblasts and epithelial cells via COL1A2-CD44 promoting the PI3K-AKT signaling pathway. Tissue sections were prepared and subjected to antigen retrieval, followed by blocking with normal ovine albumin (ZSGB-BIO, ZLI-9056). Primary antibodies, including KRT14 (ThermoFisher, MA5-11599) for epithelial cells, FN1 (Proteintech, 15613-1-AP) for fibroblasts, COL1A2 (Abcam, b96723), CD44 (ThermoFisher, 14-0441-82), and PIK3R1 (Proteintech, 60225-1-Ig) for PI3K-AKT pathway analysis, were applied overnight at 4 °C. Fluorescence-conjugated secondary antibodies were used to visualize the primary antibody binding, with

DAPI staining for nuclear visualization. Fluorescence microscopy was employed to capture images of distinct fluorophore signals, which were then analyzed to assess co-localization and pathway activation. This method enabled us to validate cell interactions and investigate the molecular mechanisms involved in HIV-ESCC tumor progression.

Results

Spatial landscape of HIV-ESCC

To characterize the spatial cellular composition of HIV-ESCC, we first employed stLearn to cluster the spatial spots based on gene expression profiles and histological similarity of each spot. Ultimately, spatial spots from patient 1 (P1) were categorized into 15 clusters, while those from patient 2 (P2) were grouped into 13 clusters. The spatial cluster distribution map illustrates that the tumor tissue of HIV-ESCC exhibits a complex cellular composition and spatial distribution, reflecting significant intra-tumoral heterogeneity. Additionally, substantial variations in cell distribution among different samples highlight pronounced inter-tumoral heterogeneity.

Based on the analysis of pathological slices (Figure S1A, B), we identified specific tissue regions. In P1, cluster 0, 1, 2, 3, 5, 6, 9, 11, 12, and 13 were designated as tumor regions, while cluster 4, 7, 8,10 and 14 were classified as peritumoral regions (Fig. 1A, B). In P2, cluster 1, 2, 3, 4, 5, 7, 8, 9, 10, 11, and 12 were identified as tumor regions, whereas cluster 0 and cluster 6 were categorized as peritumoral regions (Fig. 1C, D). The UMAP clustering diagram demonstrates a clear separation between the tumor region spots and the peritumoral region spots in both samples, highlighting the significant differences between HIV-ESCC tumor tissue and adjacent tissue. However, we also observed that the spots at the tumor boundary regions (cluster 11 and 12 in P1; cluster 1 and 3 in P2) (Fig. 1A, C) were clustered between the tumor and peritumoral regions, suggesting a potential intermediate state from normal to tumor.

To assess the spatial distribution of cell types in HIV-ESCC, we first utilized ESTIMATE to calculate the stromal scores for each cluster, providing a rough estimate of stromal cell proportions. The results indicated that cluster 2 and 5 in P1 exhibited lower stromal scores, while the stromal scores for each cluster in P2 were relatively

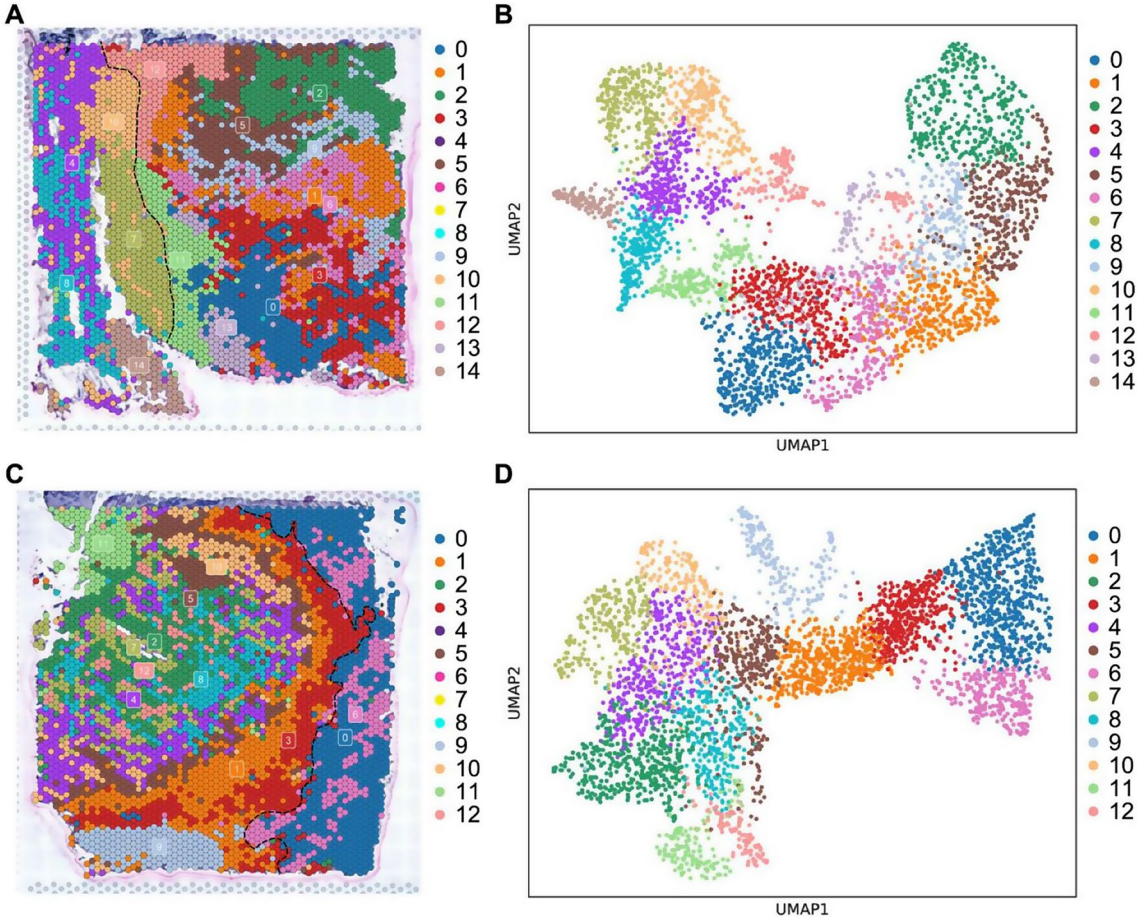

Fig. 1 (**A**) Spatial distribution and (**B**) UMAP of clusters in P1; (**C**) Spatial distribution and (**D**) UMAP of clusters in P2

uniform (Fig. 2A, B). Furthermore, we calculated tumor purity for each spot based on the ESTIMATE scores, reflecting the proportion of tumor epithelial cells, which exhibited an opposite trend compared to the stromal scores (Figure S1C, D).

To further elucidate the composition of different cell types in each spot, we collected classic cell marker genes from existing literature and statistically analyzed their expression across the spots. The results revealed that EPCAM, a widely used gene for epithelial cell annotation, was expressed at significantly lower levels in HIV-ESCC compared to other maker genes of epithelial cell such as SFN and KRT14 (Fig. 2C, D). Kimura et al. found that the survival rates of patients with tumors with high EPCAM expression was significantly higher than those for patients with tumors with low EPCAM expression [27]. And Driemel et; al. showed that low EPCAM phenotype was associated with migration, invasion and dissemination of esophageal cancer [28]. This suggest that HIV-ESCC might have a higher degree of malignancy. Moreover, the cell types indicated by the marker genes were consistent with the ESTIMATE estimates. In P1, cluster 2 and cluster 5 were predominantly composed of epithelial cells, whereas clusters 0 and 7 contained a higher proportion of fibroblasts. In contrast, cluster 2 in P2 exhibited a greater abundance of fibroblasts, while the distribution of epithelial cells was relatively uniform across different clusters. Furthermore, both epithelial and fibroblast marker genes were expressed in all the clusters, suggesting a mixed presence of these two cell types in HIV-ESCC, indicating that they tend to be mixed with each other rather than clustered independently in HIV-ESCC. Additionally, the abundance of marker genes indicates a small population of endothelial cells is present in HIV-ESCC, primarily located in the peritumoral tissues (cluster 10 in P1 and cluster 6 in P2).

To validate these findings through an alternative approach, we downloaded publicly available single-cell sequencing data for ESCC [23] as reference data and employed CARD to perform deconvolution analysis on our spatial transcriptomics data. This analysis provided a rough estimate of the proportions of different cell types in each spot. The results indicated that the primary cell types in HIV-ESCC tumor tissue are epithelial cells and fibroblasts, with a minor presence of endothelial cells, while the proportions of other cell types were very low (Figure S2A, B). Additionally, the cell proportion statistics revealed that specific spots consist entirely of epithelial cells (e.g., cluster 2 and cluster 5 in P1, as well as certain spots in cluster 7, 11, and cluster 12 in P2), whereas most of other spots contain both epithelial cells and fibroblasts. This observation reinforces the notion that a mixed spatial distribution of epithelial cells and fibroblasts is characteristic of HIV-ESCC (Figure S2C-F).

Meanwhile, the results from inferCNV also showed that clusters with a higher proportion of epithelial cells had more CNV (Figure S2G, H). To verify the analysis results, combined with the existing literature and analysis results, we selected FN1 and KRT14 as markers of fibroblasts and epithelial cells respectively, and verified the distribution of these two populations in HIV-ESCC with multiplex immunofluorescence assay. The results confirmed that fibroblasts in HIV-ESCC were highly infiltrated and widely distributed in tumor tissues, and mixed with epithelial cells, which was consistent with the analysis results (Fig. 2E; Figure S3). To determine whether the extensive mixing of these two cell types is unique to HIV-ESCC or common across all ESCC cases, we reviewed existing spatial transcriptomics studies on ESCC. And we found that in Guo's study, tumor regions and stromal regions are enriched with epithelial cells and stromal cells, respectively, without significant mixing [18]. This may indicate that the extensive integration of fibroblasts with epithelial cells in tumor tissue is specific to HIV- ESCC.

Immune microenvironment of HIV-ESCC

HIV infection alters the immune environment within affected patients. To explore the tumor microenvironment of HIV-ESCC, we first evaluated the immune scores for each spatial spot. The results indicated that clusters 1, 2, 5, and 9 in P1 — characterized by a higher proportion of epithelial cells — exhibited relatively lower immune scores (Fig. 3A). However, there seems no differences between the different clusters in P2 (Fig. 3B).

To assess the infiltration of immune cells in HIV-ESCC, we conducted a statistical analysis of the expression levels of classic marker genes for various immune cell types. Our findings revealed that classic marker genes associated with myeloid cells, such as FCGR3A, LYZ, and CD14, were expressed in HIV-ESCC tissue, while marker genes for B cells, T cells, and NK cells showed minimal to no expression (Figure S4A, B). This indicates that myeloid cells might be the predominant immune cell type present in HIV-ESCC tissue, with a notable absence of other immune cell populations. At the same time, we observed that almost all immune cell marker genes were not expressed in cluster 1, 2, 5, and 9 of P1, which was consistent with the ESTIMATE results.

To further delineate the myeloid cell types in HIV-ESCC, we analyzed the expression levels of several known molecular marker genes. The results demonstrated that macrophages are the dominant subtype of myeloid cells in HIV-ESCC tissue, as indicated by the presence of marker genes such as CD14, FCGR3A, and CD68 (Fig. 3C, D). Additionally, two monocyte marker genes, EREG and IL1B, were relatively highly expressed in cluster 2, cluster 5, and cluster 9 of P1, as well as in

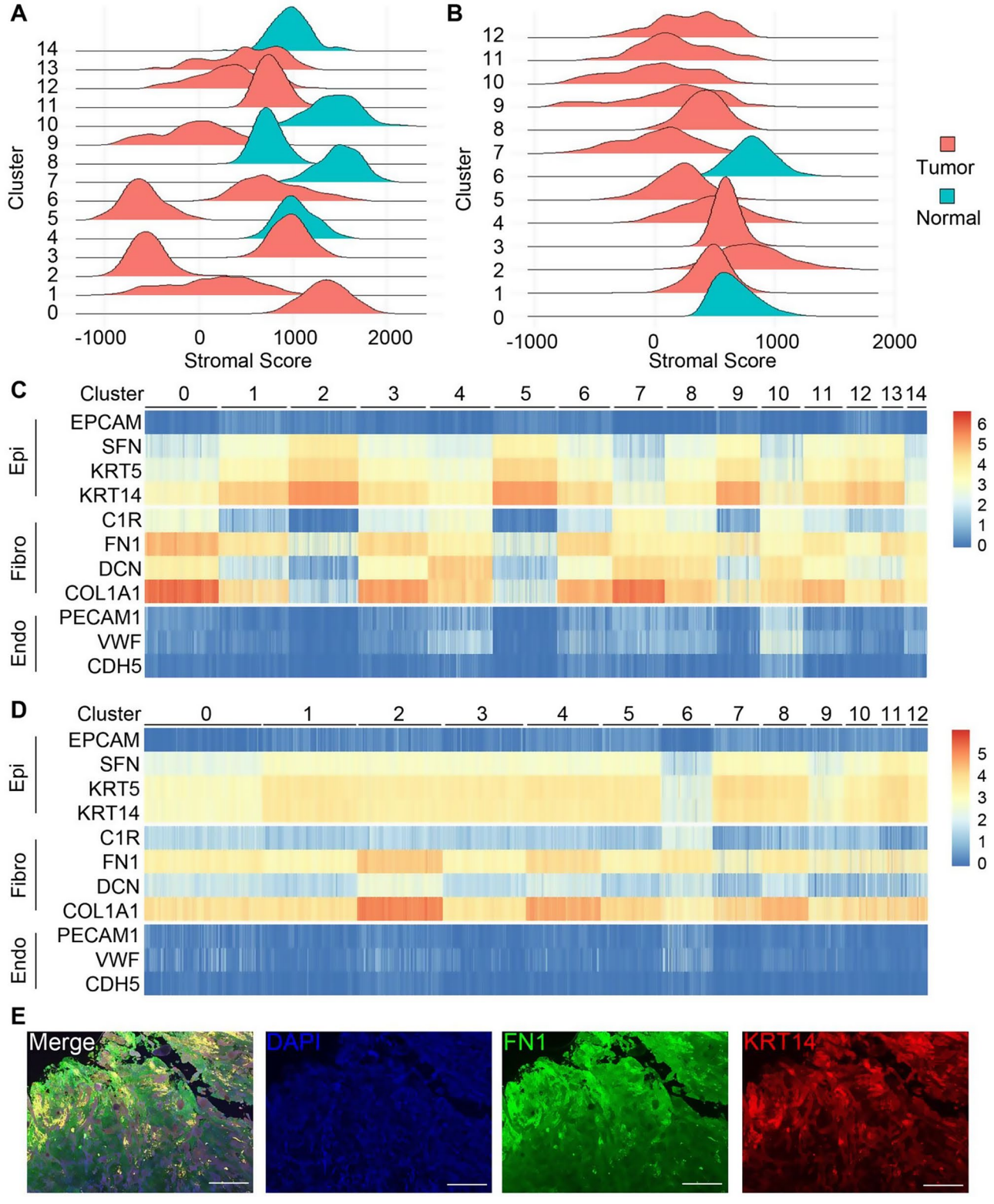

Fig. 2 Stromal score of each cluster in (**A**) P1 and (**B**) P2; Heatmap of marker genes of epithelial (Epi), fibroblast (Fibro) and endothelial (Endo) cells in each cluster in (**C**) P1 and (**D**) P2; (**E**) Multiplex immunofluorescence staining of FN1 and KRT14 in tumor tissues of HIV-ESCC. Nuclei labeled with DAPI (blue), FN1 (green), KRT14 (red). Scale bar, 500 μm

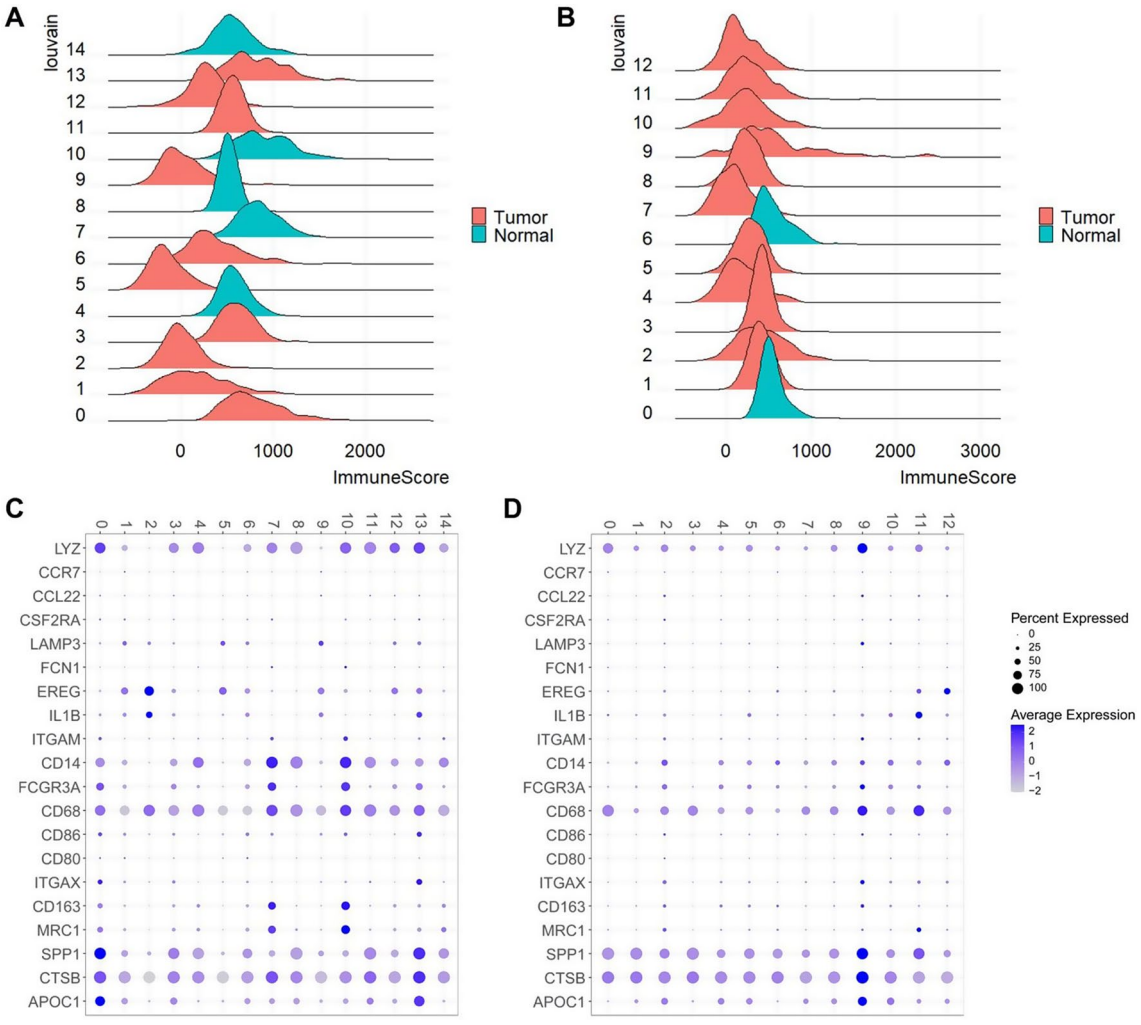

Fig. 3 Immune score of each cluster in (**A**) P1 and (**B**) P2; Dot plot of mean expression of canonical marker genes for myeloid cell types of (**C**) P1 and (**D**) P2

cluster 11 and cluster 12 of P2, which coincidentally correspond to clusters with a higher proportion of tumor epithelial cells. This suggests a potential interactive relationship between monocytes and tumor epithelial cells. In contrast, the marker genes for dendritic cells (DCs) were almost undetectable.

Further statistics showed that M1-type macrophage marker genes were almost undetected, while M2-type macrophage marker genes CD163 and MRC1 were rarely expressed in clusters except in the para-cancerous regions adjacent to the tumor tissue in P1 (cluster 7 and 10). He et al. observed a barrier between α-SMA$^+$ fibroblasts and CD163$^+$ macrophages (M2-type macrophage) in some ESCC invasion front areas [29]. The results may point to the presence of an immune cell barrier in P1, while P2 does not. At the same time, we found that SPP1$^+$ macrophages were enriched in the tumor tissues of both HIV-ESCC samples, and SPP1$^+$ macrophages have been reported to have immunosuppressive and tumor promoting effects [30, 31]. These observations might indicate a dysfunctional immune microenvironment in HIV-ESCC. At the same time, it has been reported that SPP1$^+$ macrophages interact with regulatory T cells (Tregs) through GALECTIN signaling to enhance the immunosuppressor environment of ESCC tumors and reduce the effect of ESCC immunotherapy [32, 33]. The enrichment of SPP1$^+$ macrophages in HIV-ESCC could potentially influence the effectiveness of immunotherapy.

In addition, the scores on genes associated with the HIV infection process showed values close to zero and showed minimal variation among clusters (Figure S4C, D). This suggests that antiviral drug control of HIV may prevent it from fully infecting tumor tissue, and regulate tumor progression by changing the state of immune cells.

Enriched communication between fibroblasts and epithelial cells through COL1A2-CD44 in HIV-ESCC

Utilizing the spatial location information provided by spatial transcriptomics, we can more effectively illustrate the interactions among cells. To reveal the key cellular communication processes in HIV-ESCC, we utilized CellChat to estimate the cell communications across various clusters. The results indicated that collagen-related pathways were enriched in both P1 and P2 samples, with the strongest communications observed between fibroblast enriched clusters, like 0, 3, and 6 in P1 and clusters 2, 4, and 8 in P2 (Fig. 4A, B), which indicated that fibroblasts in these regions communicate with other cells through collagen secretion.

To further validate these results, we conducted a significance analysis of the LR pairs involved in cellular communication using stLearn. The results indicated that the top-ranked significant LR pairs in both samples were collagen-related genes and their receptor proteins, with the interactions between COL1A2 and CD44, as well as ITGB1, being particularly pronounced (Fig. 4C, D). Further analysis of LR potential indicated that the interaction between COL1A2 and CD44 was particularly prominent in HIV-ESCC, with significant interactions observed within P1: cluster 0 - cluster 0, cluster 1 - cluster 1, cluster 3 - cluster 3, cluster 6 - cluster 1, and cluster 6 - cluster 6 (Fig. 4E). In P2, the most significant interactions included cluster 2 - cluster 2, cluster 2 - cluster 7, cluster 2 - cluster 8, cluster 2 - cluster 12, cluster 4 - cluster 4, cluster 4 - cluster 7, cluster 7 - cluster 7, and cluster 8 - cluster 8 (Fig. 4F). These results suggest that the most significant LR interactions occur primarily within the same clusters, although other significant interacting clusters are also spatially proximate (for example, cluster 1 and 6 in P1; cluster 2 with clusters 7 and 8, as well as cluster 4 with clusters 7 and 8 in P2). This indicates that the interaction between COL1A2 and CD44 is more likely to involve direct cell-to-cell contact rather than long-range signaling. Additionally, these significant interacting clusters exhibited high expression levels of both fibroblast and tumor epithelial cell marker genes, suggesting a higher abundance of both cell types in these regions.

To compare our findings with those from ordinary non-HIV-associated ESCC, we also analyzed those reported key cell communication LR pairs in our HIV-ESCC samples. For example, Chen et al. reported that interactions between ESCC epithelial cells through EFNB1-EPHB4 promote epithelial-mesenchymal transition and cell proliferation [34]. Our analysis also revealed that the EFNB1-EPHB4 interaction was significant within epithelial cell clusters in HIV-ESCC samples (Fig. 4E, F), indicating the similar EFNB1-EPHB4 interaction among epithelial cells in HIV-ESCC; however, its potential role significantly weaker than that of COL1A2-CD44 interaction. At the same time, Jia et al. discovered significant interactions of COL4A2-SDC1 in ESCC [35], and the interactions of MIF-(CD74 + CD44) found in studies by Guo et al. [18] and He et al. [29] were also detected in HIV-ESCC. These findings suggest that these LR interactions are commonly present in ESCC. However, their interaction strength in HIV-ESCC is not as strong as that of COL1A2-CD44, indicating that the significant interaction of COL1A2-CD44 may be unique to HIV-ESCC.

At the same time, we found that in the TCGA data, both COL1A2 and CD44 were significantly up-regulated in esophagus cancer (Figure S5A, B), and COL1A2 was significantly correlated with disease-free survival of ESCA, and patients with high expression of COL1A2 had worse disease-free survival (Figure S5C). All these findings suggest that COL1A2 and CD44 can promote the malignant progression of esophagus cancer.

Overall, these results might indicate that in HIV-ESCC, fibroblasts and tumor epithelial cells are mixed and enriched in certain regions, where fibroblasts interact with tumor epithelial cells through the COL1A2-CD44 pair, influencing tumor progression.

COL1A2+ fibroblasts activate the PI3K-AKT signaling pathway of CD44+ epithelial cells

To investigate the effects of fibroblasts on tumor epithelial cells via the COL1A2-CD44 LR pair, we further screened for significant spots based on LR score and p-value (p-value < 0.05), classifying the remaining spots as non-significant (Fig. 5A-F). We then conducted differential gene expression analysis between significant and non-significant spots for both samples. In total, 336 genes were upregulated in the significant spots of sample P1, while 329 genes were upregulated in the significant spots of sample P2, with 170 genes showing upregulation in both samples (Fig. 5G; Figure S5D, E). Fibroblast related genes such as COL1A1, COL3A1, FN1 and LUM were up-regulated in spots with significant interaction. In addition, ADAM12 and POSTN, which were reported to promote ESCC metastasis and invasion, were also up-regulated in these spots [36, 37]. KEGG functional enrichment analysis revealed that these commonly upregulated genes were primarily enriched in pathways related to protein digestion and absorption, muscle cell cytoskeleton, and cell adhesion, all of which are associated with collagen genes (Fig. 5H). Additionally, the PI3K-AKT signaling pathway was also enriched, an important signaling pathway in ESCC linked to its progression [38]. Based on these findings, we hypothesize that in HIV-ESCC, fibroblasts interact with epithelial cells through the COL1A2-CD44 pair, thereby activating the PI3K-AKT signaling pathway and subsequently promoting tumor progression in HIV-ESCC.

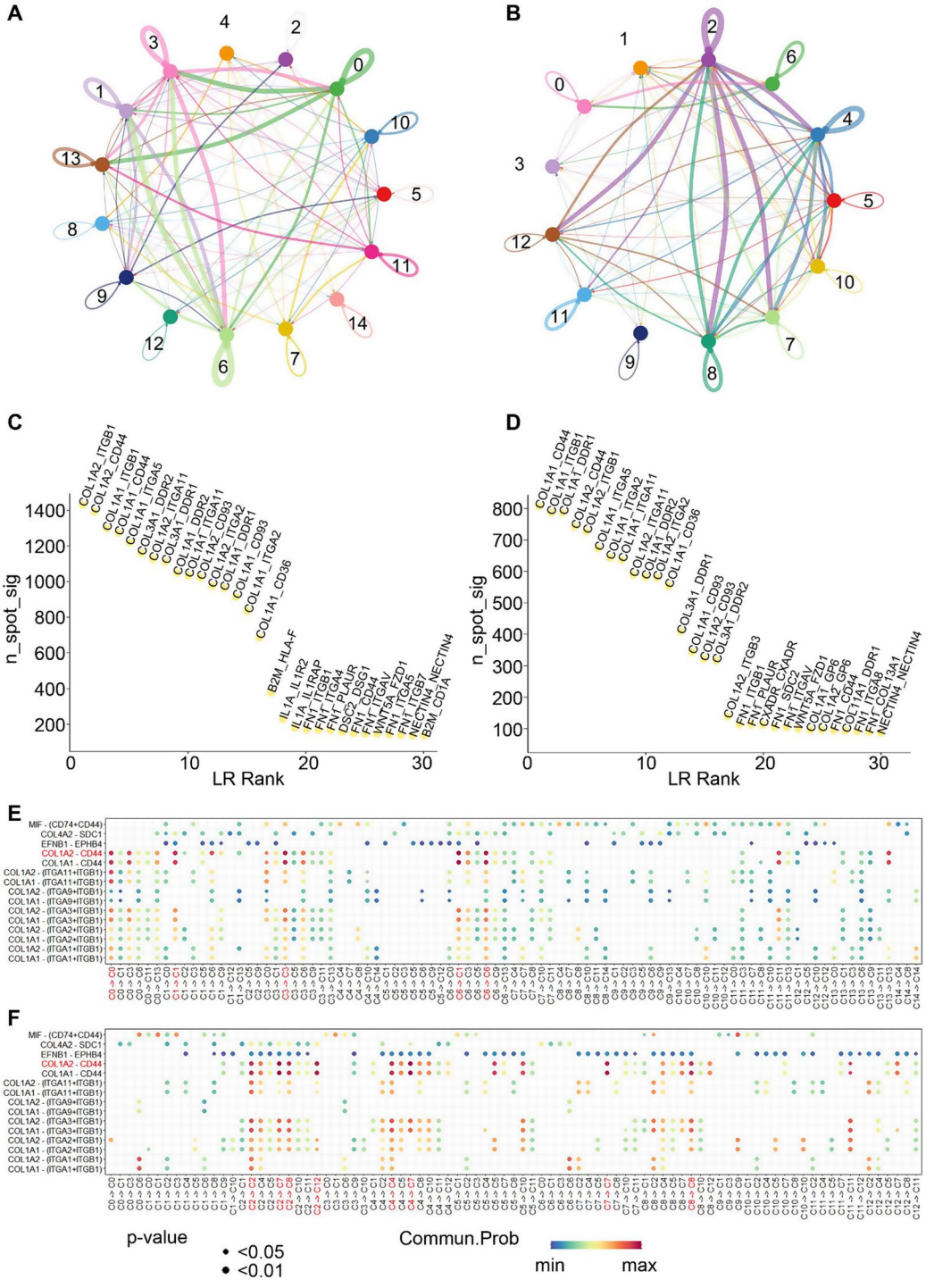

Fig. 4 Circle plot showing the intercellular communication network of collagen pathways in (**A**) P1 and (**B**) P2, where the edge thickness represents the strength of the interaction. Top 30 ligand-receptor pairs in (**C**) P1 and (**D**) P2; The enriched signaling ligand–receptor pairs between clusters in (**E**) P1 and (**F**) P2

Further, we found that the expression of PIK3R1, a key gene in the PI3K-AKT signaling pathway, was elevated in spots with significant interaction (Figure S5F). To verify this result, we collected another 6 samples of HIV-ESCC tumor tissue and simultaneously detected COL1A2, CD44 and PIK3R1 using multiplex immunofluorescence assay (Fig. 5I; Figure S6). The results showed that COL1A2 and CD44 were very close to each other in some regions of HIV-ESCC. Moreover, PIK3R1 and CD44 show high colocalization properties. These results

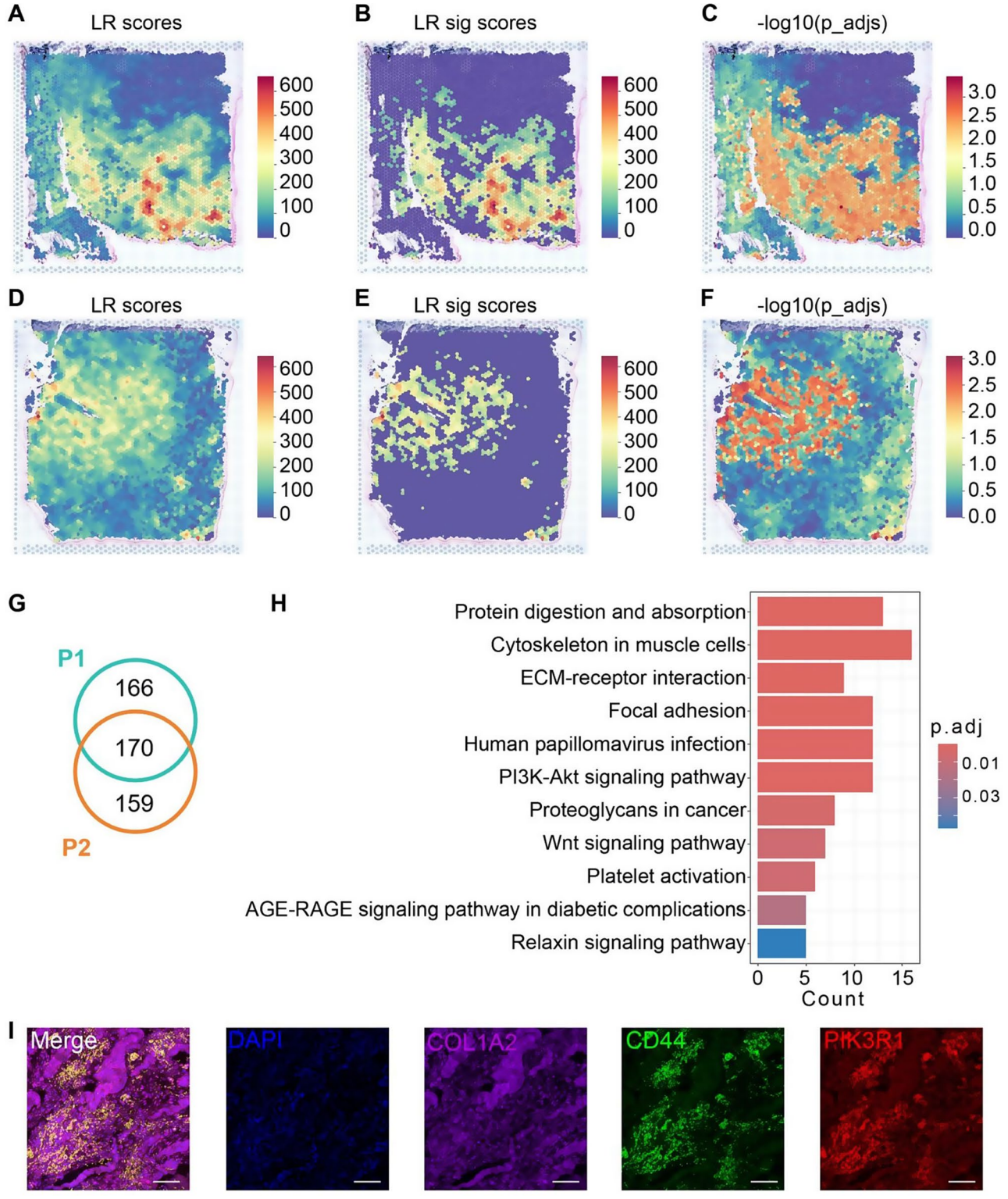

Fig. 5 (**A**) LR scores of spots; (**B**) LR scores of significant spots (p_value < 0.05); (**C**) -log10(p_adjs) of spots in P1; (**D**) LR scores of spots; (**E**) LR scores of significant spots (p_value < 0.05); (**F**) -log10(p_adjs) of spots in P2; (**G**) Venn plot showing the number of upregulation genes in significant spots within P1 and P2; (**H**) Enriched KEGG pathways of the common 170 upregulated genes in the significant spots of P1 and P2; (**I**) Multiplex immunofluorescence staining of COL1A2, CD44 and PIK3R1 in tumor tissues of HIV-ESCC. Nuclei labeled with DAPI (blue), COL1A2 (purple), CD44 (green), PIK3R1 (red). Scale bar, 100 μm

might indicate that tumor fibroblasts with high expression of COL1A2 interact with tumor epithelial cells with high expression of CD44, promoting the high expression of PIK3R1 in these cells, thus activating the PI3K-AKT signaling pathway and ultimately promoting the progression of HIV-ESCC.

Discussion

HIV infection remains a global health challenge. Although HAART can control HIV and extend the life expectancy of individuals, it has transformed HIV into a chronic disease. With the increased survival rate of people living with HIV, other health concerns have emerged, Including a rising incidence of various diseases, particularly cancers. Detrimental effects of HIV on the immune system alter the immune microenvironment in tissues, which may influence tumor development and progression.

In this study, we used spatial transcriptome technology to analyze HIV-ESCC, which has a high prevalence among HIV-infected peoples. Our goal was to explore the unique tumor microenvironment for HIV-ESCC at the spatial cellular level. It was found that fibroblasts and epithelial cells were mainly distributed in HIV-ESCC tumor tissues, with these two cell types often interspersed, rather than clearly delineated. Although previous studies have suggested that HIV promotes tissue fibrosis, the specific relationship between HIV and fibroblast accumulation in HIV-ESCC remains poorly understood and warrants further investigation.

Besides, the results of cell communication analysis showed that these interlaced fibroblasts had strong cell communication with epithelial cells. Fibroblasts interacted with $CD44^+$ epithelial cells by secreting COL1A2. This interaction up-regulated the expression of the key gene PIK3R1 in $CD44^+$ epithelial cells, activating the PI3K-AKT signaling pathway, which plays a critical role in driving HIV-ESCC tumor progression. The discovery of the cellular molecular mechanism reveals the special molecular mechanism of HIV-ESCC tumor progression.

In addition, the analysis of the immune microenvironment showed limited immune cell infiltration in HIV-ESCC tumors, and most immune cells were scarce. Only a small population of $SPP1^+$ macrophages were detected in tumor tissues, which contributes to the immunosuppressive environment within the tumor. This not only diminished the efficacy of immunotherapy [32, 33], but also promoted the survival and metastasis of tumor cells [39, 40]. Furthermore, it has been confirmed that HIV infection of macrophages can lead to the up-regulation of SPP1 expression in macrophages, and lead to the significant enhancement of HIV infectibility and replication [41]. In conclusion, these findings suggest that even though antiviral treatment can stabilize the disease of HIV-infected people, HIV continues to influence tumor progression by altering the immune landscape, leading to changes in the HIV-ESCC tumor microenvironment.

Conclusions

This study confirmed the extensive infiltration of fibroblasts in HIV-ESCC and their tendency to fully mix with epithelial cells. Meanwhile, HIV-ESCC is characterized by a compromised immune microenvironment. Mechanistically, we found that mixed fibroblasts in HIV-ESCC strongly interact with epithelial cells, particularly through COL1A2-CD44 ligand-receptor pairs. This interaction activates the PI3K-AKT pathway in tumor epithelial cells, thereby promoting the progression of HIV-ESCC.

Abbreviations

CNV	Copy Number Variation
DC	Dendritic Cell
ESCA	Esophagus Cancer
ESCC	Esophageal Squamous Cell Carcinoma
HAART	Highly Active Antiretroviral Therapy
H&E	Hematoxylin and eosin
HIV	Human Immunodeficiency Virus
HIV-ESCC	Esophageal Squamous Cell Carcinoma with HIV Infection
KEGG	Kyoto Encyclopedia of Genes and Genomes
LR	Ligand-Receptor
PLWH	People Living with HIV
SME	Spatial Morphological Extraction
Tregs	Regulatory T Cells
UMAP	Uniform Manifold Approximation and Projection

Supplementary Information

The online version contains supplementary material available at https://doi.org/10.1186/s12943-025-02248-3.

Supplementary Material 1

Acknowledgements

We'd like to thank Prof. Chen Wu from National Cancer Center/Cancer Hospital, Chinese Academy of Medical Sciences and Peking Union Medical College, to provide the scRNA-seq data of ESCC.

Author contributions

Y.P. and X.Y. designed and supervised this study, and revised the manuscript; Y.Z. and Y.J. performed data analysis and wrote the manuscript; G.L. collected patients' samples; Y.M. performed multiplex immunofluorescence assay; T.F. and Y.P. helped to perform data analysis.

Funding

This study is supported by National Natural Science Foundation of China (U24A20721, 32100524) and the 1.3.5 Project for Disciplines of Excellence, West China Hospital of Sichuan University (ZYGD23027).

Data availability

No datasets were generated or analysed during the current study.

Declarations

Ethics approval and consent to participate

The study was performed in accordance with the declaration of Helsinki. Human HIV-ESCC samples were obtained from The Public Health Clinical Center of Chengdu under protocols approved by the Ethics Committee. Written informed consent was obtained from each patient.

Consent for publication
We have obtained consents to publish this paper from all participants of this study.

Competing interests
The authors declare no competing interests.

Received: 2 December 2024 / Accepted: 27 January 2025
Published online: 25 February 2025

References

1. Margolis DM, Archin NM, Cohen MS, Eron JJ, Ferrari G, Garcia JV, Gay CL, Goonetilleke N, Joseph SB, Swanstrom R, et al. Curing HIV: seeking to target and clear persistent infection. Cell. 2020;181:189–206.
2. Singh S, Kirk O, Jaffar S, Karakezi C, Ramaiya K, Kallestrup P, Kraef C. Patient perspectives on integrated healthcare for HIV, hypertension and type 2 diabetes: a scoping review. BMJ Open. 2021;11:e054629.
3. Shmakova A, Germini D, Vassetzky Y. HIV-1, HAART and cancer: a complex relationship. Int J Cancer. 2020;146:2666–79.
4. Carbone A, Vaccher E, Gloghini A. Hematologic cancers in individuals infected by HIV. Blood. 2022;139:995–1012.
5. Mremi A, Mswima J, Mlay MG, Bartholomew H, Alloyce JP, Mmbaga BT, Bartlett J. Cancer spectrum in HIV-infected patients: a zonal hospital experience in Tanzania. Cancer Treat Res Commun. 2020;25:100213.
6. Gopal S, Krysiak R, Liomba NG, Horner MJ, Shores CG, Alide N, Kamiza S, Kampani C, Chimzimu F, Fedoriw Y, et al. Early experience after developing a pathology laboratory in Malawi, with emphasis on cancer diagnoses. PLoS ONE. 2013;8:e70361.
7. Sung H, Ferlay J, Siegel RL, Laversanne M, Soerjomataram I, Jemal A, Bray F. Global Cancer statistics 2020: GLOBOCAN estimates of incidence and Mortality Worldwide for 36 cancers in 185 countries. CA Cancer J Clin. 2021;71:209–49.
8. Chen W, Zheng R, Baade PD, Zhang S, Zeng H, Bray F, Jemal A, Yu XQ, He J. Cancer statistics in China, 2015. CA Cancer J Clin. 2016;66:115–32.
9. Enzinger PC, Mayer RJ. Esophageal cancer. N Engl J Med. 2003;349:2241–52.
10. Jensen BE, Oette M, Haes J, Haussinger D. HIV-Associated Gastrointestinal Cancer. Oncol Res Treat. 2017;40:115–8.
11. Kayamba V, Bateman AC, Asombang AW, Shibemba A, Zyambo K, Banda T, Soko R, Kelly P. HIV infection and domestic smoke exposure, but not human papillomavirus, are risk factors for esophageal squamous cell carcinoma in Zambia: a case-control study. Cancer Med. 2015;4:588–95.
12. Thrift AP, Kramer JR, Hartman CM, Royse K, Richardson P, Dong Y, Raychaudhury S, Desiderio R, Sanchez D, Anandasabapathy S, et al. Risk and predictors of esophageal and stomach cancers in HIV-Infected veterans: a matched cohort study. J Acquir Immune Defic Syndr. 2019;81:e65–72.
13. Szychowiak P, Boulain T, Timsit JF, Elabbadi A, Argaud L, Ehrmann S, Issa N, Canet E, Martino F, Bruneel F, et al. Clinical spectrum and prognostic impact of cancer in critically ill patients with HIV: a multicentre cohort study. Ann Intensive Care. 2023;13:74.
14. Salahuddin S, Cohen O, Wu M, Perez Irizarry J, Vega T, Gan G, Deng Y, Isaeva N, Prasad M, Schalper KA, et al. Human immunodeficiency virus is Associated with Poor overall survival among patients with Head and Neck Cancer. Clin Infect Dis. 2023;76:1449–58.
15. Wistuba II, Behrens C, Milchgrub S, Virmani AK, Jagirdar J, Thomas B, Ioachim HL, Litzky LA, Brambilla EM, Minna JD, Gazdar AF. Comparison of molecular changes in lung cancers in HIV-positive and HIV-indeterminate subjects. JAMA. 1998;279:1554–9.
16. Calkins KL, Chander G, Joshu CE, Visvanathan K, Fojo AT, Lesko CR, Moore RD, Lau B. Immune Status and Associated Mortality after Cancer Treatment among individuals with HIV in the antiretroviral therapy era. JAMA Oncol. 2020;6:227–35.
17. Pinato DJ, Kaneko T, D'Alessio A, Forner A, Fessas P, Minguez B, Giannini EG, Grillo F, Diaz A, Mauri FA, et al. Integrated phenotyping of the anti-cancer immune response in HIV-associated hepatocellular carcinoma. JHEP Rep. 2023;5:100741.
18. Guo W, Zhou B, Yang Z, Liu X, Huai Q, Guo L, Xue X, Tan F, Li Y, Xue Q, et al. Integrating microarray-based spatial transcriptomics and single-cell RNA-sequencing reveals tissue architecture in esophageal squamous cell carcinoma. EBioMedicine. 2022;84:104281.
19. Liu X, Zhao S, Wang K, Zhou L, Jiang M, Gao Y, Yang R, Yan S, Zhang W, Lu B, et al. Spatial transcriptomics analysis of esophageal squamous precancerous lesions and their progression to esophageal cancer. Nat Commun. 2023;14:4779.
20. Pham D, Tan X, Balderson B, Xu J, Grice LF, Yoon S, Willis EF, Tran M, Lam PY, Raghubar A, et al. Robust mapping of spatiotemporal trajectories and cell-cell interactions in healthy and diseased tissues. Nat Commun. 2023;14:7739.
21. Wu R, Guo W, Qiu X, Wang S, Sui C, Lian Q, Wu J, Shan Y, Yang Z, Yang S, et al. Comprehensive analysis of spatial architecture in primary liver cancer. Sci Adv. 2021;7:eabg3750.
22. Yoshihara K, Shahmoradgoli M, Martinez E, Vegesna R, Kim H, Torres-Garcia W, Trevino V, Shen H, Laird PW, Levine DA, et al. Inferring tumour purity and stromal and immune cell admixture from expression data. Nat Commun. 2013;4:2612.
23. Zhang X, Peng L, Luo Y, Zhang S, Pu Y, Chen Y, Guo W, Yao J, Shao M, Fan W, et al. Dissecting esophageal squamous-cell carcinoma ecosystem by single-cell transcriptomic analysis. Nat Commun. 2021;12:5291.
24. Ma Y, Zhou X. Spatially informed cell-type deconvolution for spatial transcriptomics. Nat Biotechnol. 2022;40:1349–59.
25. Jin S, Guerrero-Juarez CF, Zhang L, Chang I, Ramos R, Kuan CH, Myung P, Plikus MV, Nie Q. Inference and analysis of cell-cell communication using CellChat. Nat Commun. 2021;12:1088.
26. Jin S, Plikus MV, Nie Q. CellChat for systematic analysis of cell-cell communication from single-cell transcriptomics. Nat Protoc. 2025; 20(1):180–219.
27. Kimura H, Kato H, Faried A, Sohda M, Nakajima M, Fukai Y, Miyazaki T, Masuda N, Fukuchi M, Kuwano H. Prognostic significance of EpCAM expression in human esophageal cancer. Int J Oncol. 2007;30:171–9.
28. Driemel C, Kremling H, Schumacher S, Will D, Wolters J, Lindenlauf N, Mack B, Baldus SA, Hoya V, Pietsch JM, et al. Context-dependent adaption of EpCAM expression in early systemic esophageal cancer. Oncogene. 2014;33:4904–15.
29. He JZ, Chen Y, Zeng FM, Huang QF, Zhang HF, Wang SH, Yu SX, Pang XX, Liu Y, Xu XE, et al. Spatial analysis of stromal signatures identifies invasive front carcinoma-associated fibroblasts as suppressors of anti-tumor immune response in esophageal cancer. J Exp Clin Cancer Res. 2023;42:136.
30. Bill R, Wirapati P, Messemaker M, Roh W, Zitti B, Duval F, Kiss M, Park JC, Saal TM, Hoelzl J, et al. CXCL9:SPP1 macrophage polarity identifies a network of cellular programs that control human cancers. Science. 2023;381:515–24.
31. Yang Z, Tian H, Chen X, Li B, Bai G, Cai Q, Xu J, Guo W, Wang S, Peng Y, et al. Single-cell sequencing reveals immune features of treatment response to neoadjuvant immunochemotherapy in esophageal squamous cell carcinoma. Nat Commun. 2024;15:9097.
32. Geng Z, Li F, Yang Z, Li B, Xu Y, Wu B, Sheng Y, Yuan P, Huang L, Qi Y. Integrative analyses of bulk and single-cell RNA-seq reveals the correlation between SPP1(+) macrophages and resistance to neoadjuvant chemoimmunotherapy in esophageal squamous cell carcinoma. Cancer Immunol Immunother. 2024;73:257.
33. Qi J, Sun H, Zhang Y, Wang Z, Xun Z, Li Z, Ding X, Bao R, Hong L, Jia W, et al. Single-cell and spatial analysis reveal interaction of FAP(+) fibroblasts and SPP1(+) macrophages in colorectal cancer. Nat Commun. 2022;13:1742.
34. Chen L, Zhu S, Liu T, Zhao X, Xiang T, Hu X, Wu C, Lin D. Aberrant epithelial cell interaction promotes esophageal squamous-cell carcinoma development and progression. Signal Transduct Target Ther. 2023;8:453.
35. Jia Y, Zhang B, Zhang C, Kwong DL, Chang Z, Li S, Wang Z, Han H, Li J, Zhong Y, et al. Single-cell transcriptomic analysis of primary and metastatic tumor ecosystems in esophageal squamous cell carcinoma. Adv Sci (Weinh). 2023;10:e2204565.
36. Luo ML, Zhou Z, Sun L, Yu L, Sun L, Liu J, Yang Z, Ran Y, Yao Y, Hu H. An ADAM12 and FAK positive feedback loop amplifies the interaction signal of tumor cells with extracellular matrix to promote esophageal cancer metastasis. Cancer Lett. 2018;422:118–28.
37. Michaylira CZ, Wong GS, Miller CG, Gutierrez CM, Nakagawa H, Hammond R, Klein-Szanto AJ, Lee JS, Kim SB, Herlyn M, et al. Periostin, a cell adhesion molecule, facilitates invasion in the tumor microenvironment and annotates a novel tumor-invasive signature in esophageal cancer. Cancer Res. 2010;70:5281–92.
38. Liu B, Zhang B, Qi J, Zhou H, Tan L, Huang J, Huang J, Fang X, Gong L, Luo J, et al. Targeting MFGE8 secreted by cancer-associated fibroblasts blocks angiogenesis and metastasis in esophageal squamous cell carcinoma. Proc Natl Acad Sci U S A. 2023;120:e2307914120.
39. Sathe A, Mason K, Grimes SM, Zhou Z, Lau BT, Bai X, Su A, Tan X, Lee H, Suarez CJ, et al. Colorectal Cancer metastases in the liver establish

immunosuppressive spatial networking between Tumor-Associated SPP1 + macrophages and fibroblasts. Clin Cancer Res. 2023;29:244–60.
40. Matusiak M, Hickey JW, van Lu IDGP, Kidzinski G, Zhu L, Colburg S, Luca DRC, Phillips B, Brubaker DJ. Spatially segregated macrophage populations predict distinct outcomes in Colon cancer. Cancer Discov. 2024;14:1418–39.
41. Deng Y, Deng Y, He X, Chu J, Zhou J, Zhang Q, Guo W, Huang P, Guan X, Tang Y, et al. Prenatal inflammation-induced NF-kappaB dyshomeostasis contributes to renin-angiotensin system over-activity resulting in prenatally programmed hypertension in offspring. Sci Rep. 2016;6:21692.

Publisher's note